

High-Performance and Stable Warm White OLEDs Based on Orange Iridium(III) Phosphors Modified with Simple Alkyl Groups

Lei Ding, Chun-Xiu Zang, Li-Li Wen, Guo-Gang Shan,* Ying Gao, Hai-Zhu Sun,* Wen-Fa Xie,* and Zhong-Min Su*

Cite This: <https://dx.doi.org/10.1021/acs.organomet.0c00472>

Read Online

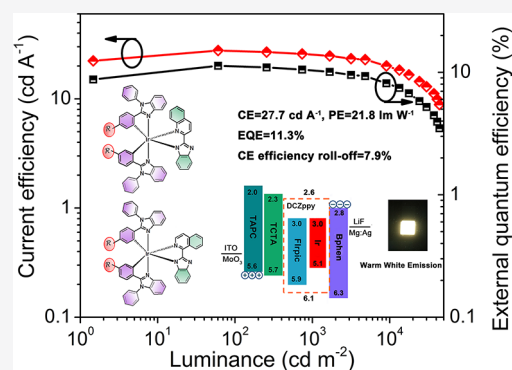
ACCESS |

Metrics & More

Article Recommendations

Supporting Information

ABSTRACT: Phosphorescent organic light-emitting diodes (OLEDs) with high electroluminescence (EL) efficiency and low efficiency roll-off are urgently required to meet the continuously increasing market need in lighting industry fields. There is an urgent demand for phosphorescent emitters with excellent photoluminescence quantum yields (PLQYs) to realize a high EL performance of OLEDs. In this work, four new orange phosphorescent iridium(III) emitters, namely Ir-1–Ir-4, were designed and synthesized successfully, in which functionalized 1,2-diphenylbenzimidazole and conjugated quinoline-benzimidazole moieties are employed as the main ligands and ancillary ligands, respectively. The obtained phosphors show relatively high efficiency and broad full width at half-maximums (FWHMs) of about 110 nm, which are favorable for constructing high-quality white OLEDs. The optimized monochromatic orange-emitting OLED of Ir-1 shows a maximum current efficiency (CE) of 27.2 cd A⁻¹, a power efficiency of 24.0 lm W⁻¹, and an external quantum efficiency (EQE) of 10.6%. A two-color OLED employing Ir-1 as the orange-emitting layer shows a maximum brightness of 43980 cd m⁻², a CE of 27.7 cd A⁻¹, a PE of 21.8 lm W⁻¹, an EQE of 11.3%, and a low CE efficiency roll-off ratio of 7.9%. Moreover, this device displays warm white emission with CIE coordinates of (0.39, 0.43) at 7 V and high color stability with a CIE variation of (0.003, 0.001).



INTRODUCTION

Currently, OLEDs have developed rapidly in the field of large-area plane display and solid-state lighting owing to their outstanding features, including flexibility, color tunability, and low power consumption.^{1–4} Phosphorescent OLEDs (PHOLEDs) based on transition-metal complexes can theoretically achieve 100% internal quantum efficiency by harvesting singlet and triplet excitons simultaneously.^{5–7} Notably, iridium(III) complexes are the most widely studied phosphorescent materials for high-performance PHOLEDs because of their encouraging properties, such as photostability, thermal stability, flexible color tunability, and short phosphorescence lifetime.⁸ Highly efficient red/orange iridium(III) complexes play an important role in the construction of high-performance full-color displays and white OLEDs.⁹ Significant improvements have been achieved in the efficiencies and stability of green PHOLEDs.^{10–12} However, the electroluminescence (EL) performance of red/orange phosphors has still fallen behind with inferior EL efficiency and efficiency roll-off at high brightness.¹³ The photoluminescence quantum yields (PLQYs) of red/orange phosphorescent emitters tend to be lower because of their narrow energy gap.^{14–16} Therefore, it is desirable to design and synthesize more efficient red/orange iridium(III) complexes with sufficient luminous efficiency for high-performance monochromatic OLEDs.

White organic light-emitting diodes (WOLEDs) for lighting applications have many issues to be addressed so that they can successfully enter the commercial market.^{17–22} Usually, WOLEDs are made up of three colors (red, green, and blue) or more to cover the whole spectrum and thus have excellent color rendering indexes (CRI).^{23–27} However, the shortcomings of complicated multilayer structure, high driving voltage, and complex synthetic method have severely limited their applications in the lighting market.²⁴ Consequently, WOLEDs comprising two colors (orange and blue) exhibit a greater potential for practical application, owing to the prominent characteristics of simpler device fabrication, lower costs, fewer masks, etc.^{28,29} However, two-color WOLEDs have higher requirements for the full width at half-maximums (FWHMs) of the phosphorescent iridium(III) complexes. In addition, most WOLEDs based on phosphors have suffered from serious efficiency roll-offs,³⁰ resulting mainly from triplet–triplet annihilation (TTA),^{14,31} unbalanced carrier

Received: July 12, 2020

distribution, and field-induced quenching. Furthermore, the EL spectra for two-color WOLEDs vary markedly under different driving voltages, leading to a great variation in the Commission Internationale de l'Éclairage (CIE) coordinates.³² Thus, efficient two-color WOLEDs with high EL efficiency, low efficiency roll-off, and good color stability are still highly desirable but remain a challenge.

To date, many red/orange iridium(III) emitters have been used to fabricate excellent performance two-color WOLEDs, providing many new molecular design concepts.^{33–35} Recently, our group reported a new orange iridium(III) complex which used 2-(1*H*-benzo[*d*]imidazol-2-yl)quinoline (HBIQ) with strong structural rigidity as an ancillary ligand. Using this complex as an orange dopant, the two-color WOLED achieved a maximum current efficiency (CE) of up to 22.1 cd A⁻¹ and maximum power efficiency (PE) of up to 25.5 lm W⁻¹. However, the two-color WOLED displays serious efficiency roll-off, which limits its practical application.³⁶ Alkyl substituents introduced on the main ligand can suppress self-quenching to some extent, thereby enhancing efficiency and dropping efficiency roll-off.³⁷ On the basis of the above discussion, in this work, the four phosphors (mPBI)₂Ir(BIQ) (**Ir-1**), (tbPBI)₂Ir(BIQ) (**Ir-2**), (mPBI)₂Ir(BISQ) (**Ir-3**), and (tbPBI)₂Ir(BISQ) (**Ir-4**) using 1-phenyl-2-*p*-tolyl-1*H*-benzo[*d*]imidazole (HmPBI) and 2-(4-*tert*-butylphenyl)-1-phenyl-1*H*-benzo[*d*]imidazole (HtbPBI) as the main ligands and rigid 2-(1*H*-benzo[*d*]imidazol-2-yl)quinoline (HBIQ) and 1-(1*H*-benzo[*d*]imidazol-2-yl)isoquinoline (HBISQ) as the ancillary ligand have been designed and characterized (Figure 1). **Ir-1** and **Ir-2** show high luminous efficiency with PLQYs of

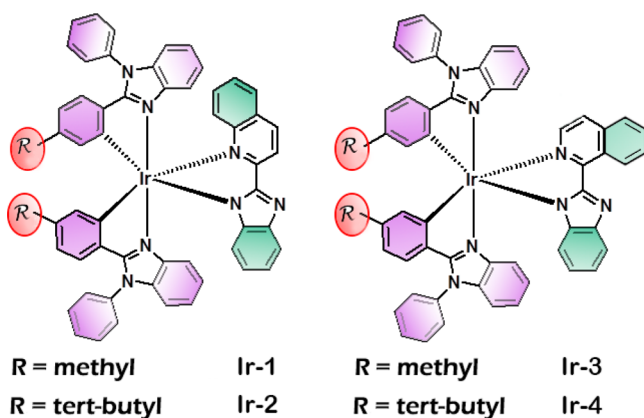


Figure 1. Chemical structures of the four orange emitters studied in this work.

up to 57.5% and 56.4% in dilute solution, respectively. The optimized orange-emitting OLED based on **Ir-1** exhibits a maximum CE of 27.2 cd A⁻¹ and an external quantum efficiency (EQE) of 10.6%. Then, two-color WOLEDs employing orange emitters were fabricated due to the broad FWHMs. **W1** exhibits warm white emission with CIE coordinates of (0.39, 0.43) at 7 V and shows a maximum brightness of 43980 cd m⁻², a highest CE of 27.7 cd A⁻¹, a highest PE of 21.8 lm W⁻¹, and a highest EQE of 11.3%. In addition, a small efficiency roll-off was achieved in **W1**. Interestingly, the device **W1** displays excellent color stability with a CIE variation of (0.003, 0.001) when the driving voltages were varied from 4 to 6 V.

RESULTS AND DISCUSSION

Syntheses. The iridium(III) complexes were prepared by the reaction of dichloro-bridged diiridium complex with the ancillary ligands HBIQ and HBISQ (Scheme 1). All crude products were purified by silica chromatography. Mass spectrometry and ¹H NMR spectroscopy were used to identify the structures of iridium(III) emitters (see Figures S1–S4 in the Supporting Information). In addition, the structures of **Ir-1**, **Ir-3**, and **Ir-4** were further confirmed by X-ray crystallography.

X-ray Crystallographic Analysis. The molecular structures of **Ir-1**, **Ir-3**, and **Ir-4** analyzed via X-ray crystallography of single crystals are illustrated in Figure 2. Single crystals were grown from a mixed solvent of CH₂Cl₂ and CH₃OH. The iridium(III) centers of these three complexes are coordinated with the same two main ligands (HmPBI or HtbPBI) and an ancillary ligand (HBIQ or HBISQ), resulting in a distorted-octahedral coordination geometry. In all cases, these molecular structures contained *trans*-nitrogen and *cis*-metalated carbon dispositions, similarly to the other previously reported analogous phosphors.^{38–40} As shown in Table S1 in the Supporting Information, the Ir1–N1 and Ir1–N3 bond lengths of all three complexes are slightly shorter than the Ir1–N5 and Ir1–N6 bond lengths due to the *trans* disposition of the main ligands. In addition, the two Ir–C bonds of **Ir-3** and **Ir-4** have almost the same length, while the Ir1–C21 bond length is longer than the Ir1–C1 bond length of **Ir-1** due to the influence of the ancillary ligand HBIQ. The bond lengths of three complexes are given in Table S1 in the Supporting Information. The detailed crystal data and structure refinement are summarized in Table S2 in the Supporting Information.

Photophysical Properties. Figure 3 shows the UV–visible absorption and PL spectra of these four complexes in dichloromethane solution at room temperature. All complexes display intense absorption bands between 230 and 350 nm assigned to π → π* transitions of cyclometalated ligands,²⁶ and the relatively weak absorption bands above 350 nm are probably related to the singlet metal to ligand charge transfer transitions (¹MLCT) and spin-forbidden metal to ligand charge transfer transitions (³MLCT).^{41,42}

At room temperature, the spectra of all phosphors reveal intense structureless emission bands. The emission maxima of **Ir-3** and **Ir-4** are red-shifted by ~15 nm in comparison to **Ir-1** and **Ir-2**, which were observed at 605, 603, 620, and 619 nm, respectively. Simultaneously, the neat films of four complexes give featureless and broadened PL spectra centered at 607, 601, 610, and 613 nm, respectively (see Figure S5 in the Supporting Information). The structureless and broad emission indicates that the emissive excited states of these complexes have predominantly ³LLCT and/or ³MLCT characters rather than ³LC characters, which often exhibit vibronically structured emission spectra.⁴³ When **Ir-1**–**Ir-4** were cooled to 77 K, the PL spectra, showing evident blue shifts relative to their spectra at room temperature, are also structureless, implying that the emissive excited-states ³LLCT and/or ³MLCT transitions play a significant role (see Figure S6 in the Supporting Information).^{44–46} As shown in Table 1, the emission lifetimes (τ) for **Ir-1**–**Ir-4** in dichloromethane solution are 0.73, 1.20, 0.50, and 1.24 μs, respectively. Emission lifetimes in the microsecond range suggest the origin of triplet emission. In addition, in degassed dichloromethane, **Ir-1** and **Ir-2** exhibit similar PLQYs of 57.5% and 56.4%,

Scheme 1. Synthetic Routes for Designed Iridium(III) Emitters

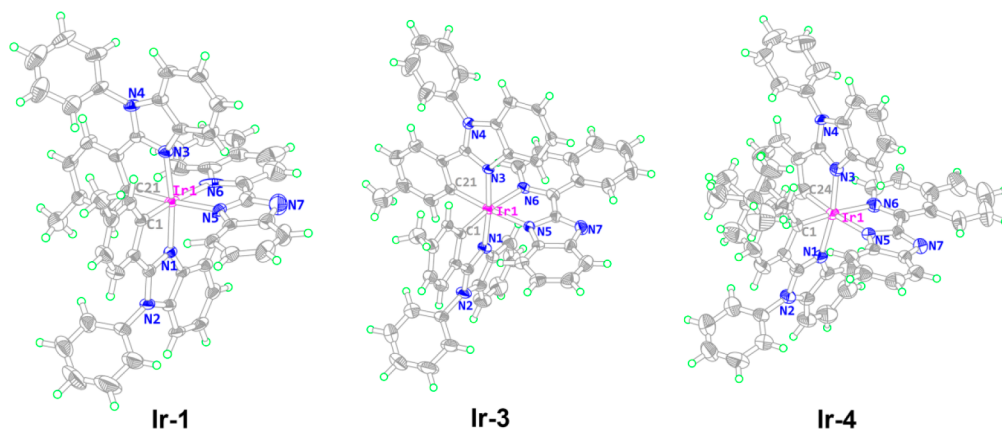
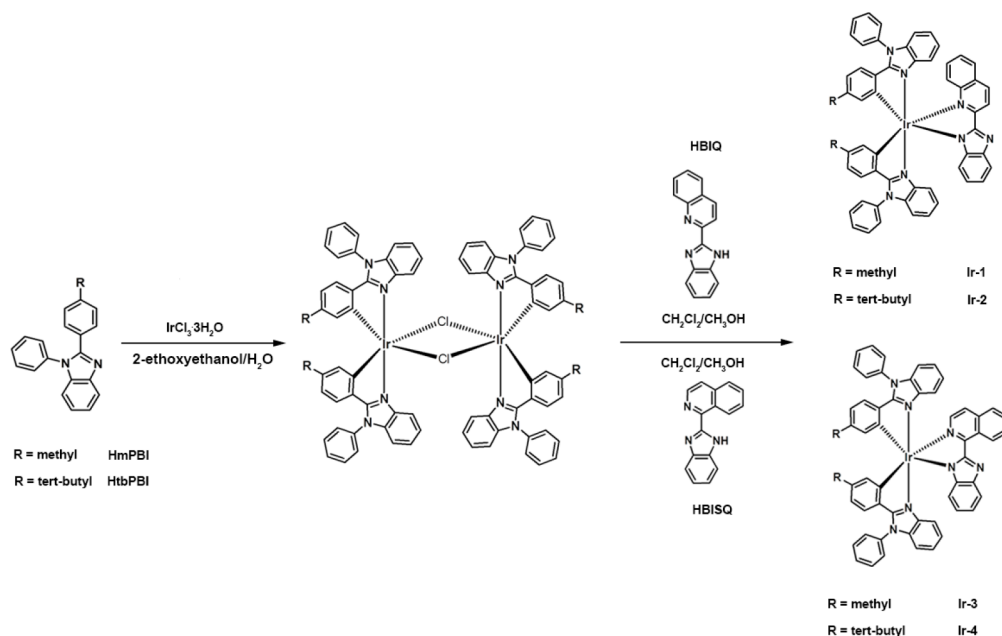


Figure 2. Single-crystal structures of three complexes with ellipsoids drawn at the 50% probability level: Ir-1 (CCDC no. 1980337), Ir-3 (CCDC no. 1969397), and Ir-4 (CCDC no. 1980338).

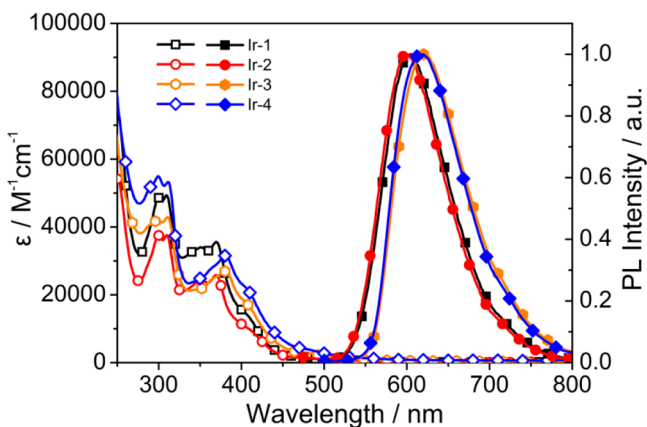


Figure 3. UV-vis and PL spectra of Ir-1–Ir-4 in dichloromethane solution with a concentration of 10^{-5} M at room temperature.

respectively, and phosphors Ir-3 and Ir-4 show relatively lower PLQYs of 32.9% and 32.0%. To gain a deeper understanding of the emission properties of all the complexes, the radiative (k_r)

and nonradiative decay rate constants (k_{nr}) were determined and are given in Table 1. k_r and k_{nr} for Ir-1 are 7.88×10^5 and 5.82×10^5 s^{-1} , for Ir-2 are 4.70×10^5 and 3.63×10^5 s^{-1} , for Ir-3 are 6.58×10^5 and 13.42×10^5 s^{-1} , and for Ir-4 are 2.58×10^5 and 5.48×10^5 s^{-1} , respectively.

Theoretical Calculations. To gain insight into the photophysical properties of all the iridium(III) complexes, the highest occupied molecular orbital (HOMO) and lowest unoccupied molecular orbital (LUMO) levels and distributions of Ir-1–Ir-4 were calculated. As shown in Figure 4, it is found that all complexes exhibit similar electronic cloud distributions, indicating that the substituents have a negligible influence on molecular orbital energy levels and distributions. The LUMOs of Ir-1–Ir-4 distributed over the ancillary ligand with a slight extension to the iridium(III) atom, while their HOMOs spread across the iridium(III) atom, the main ligands, and the ancillary ligand. The triplet excited states (T_1) were calculated to understand the emission characteristics. As shown in Table S3, the T_1 of Ir-1 and Ir-2 were almost a HOMO \rightarrow LUMO transition (90%), and the T_1 of Ir-3 and Ir-4 were mainly a HOMO \rightarrow LUMO transition (71% for Ir-3, 72% for Ir-4),

Table 1. Electrochemical and Photophysical Data for Ir-1–Ir-4

complex	$\lambda_{\text{PL,max}}^{a-c}$ (nm)	τ^a (μs)	$E_{\text{ox}}(\text{onset})^d$ (V)	E_g^e (eV)	HOMO ^f /LUMO ^g (eV)	Φ_p^{ac} (%)	k_r^h (10^5 s^{-1})	k_{nr}^h (10^5 s^{-1})
Ir-1	605, 581, 607	0.73	0.39	2.17	−5.19/−3.02	57.5, 38.4	7.88	5.82
Ir-2	603, 572, 601	1.20	0.38	2.18	−5.18/−3.00	56.4, 12.0	4.70	3.63
Ir-3	620, 602, 610	0.50	0.37	2.07	−5.17/−3.10	32.9, 32.4	6.58	13.42
Ir-4	619, 605, 613	1.24	0.35	2.11	−5.15/−3.04	32.0, 29.5	2.58	5.48

^aIr-1–Ir-4 measurements were performed in dichloromethane solution (10^{-5} M) at room temperature. ^bIr-1–Ir-4 measurements were measured in 10^{-5} M dichloromethane at 77 K. ^cMeasured in the neat film at room temperature. ^dMeasured by CV with ferrocene as the standard. ^eEstimated from the UV–vis absorption spectra. ^fObtained from the onset oxidation potentials according to $\text{HOMO} = -E_{\text{ox}}(\text{onset}) + 4.8 \text{ eV}$. ^gObtained according to $\text{LUMO} = \text{HOMO} + E_g$. ^hCalculated from τ and Φ ($k_r = \Phi/\tau$, $k_{\text{nr}} = (1 - \Phi)/\tau$).

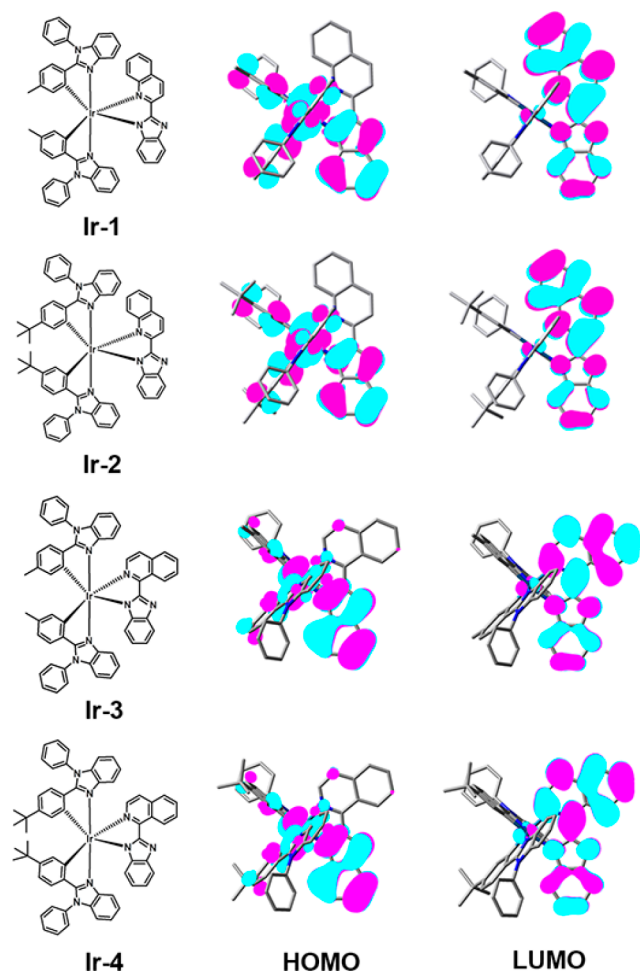


Figure 4. HOMO and LUMO distributions of Ir-1–Ir-4 (isocontour 0.02).

indicating that their T_1 emission contains a mixture of $^3\text{MLCT}$ and $^3\text{LLCT}$ (see the Supporting Information).

Electrochemical Properties. The electrochemical properties of the four phosphors have been studied by cyclic voltammetry (CV), and the corresponding data are shown in Figure 5 and Table 1. The energy gaps for Ir-1–Ir-4 were calculated to be 2.17, 2.18, 2.07, and 2.11 eV, respectively, and so it is reasonable that iridium(III) complexes could show orange emissions. Using the ferrocene/ferrocenium (Fc/Fc^+) pair as a reference, the $E_{\text{ox}}(\text{onset})$ values are 0.39, 0.38, 0.37, and 0.35 V for Ir-1–Ir-4, respectively. Their HOMO energy levels were deduced to be −5.19, −5.18, −5.17, and −5.15 eV, respectively according to the $E_{\text{ox}}(\text{onset})$ values. Consequently, the corresponding LUMO energy levels were calculated to be

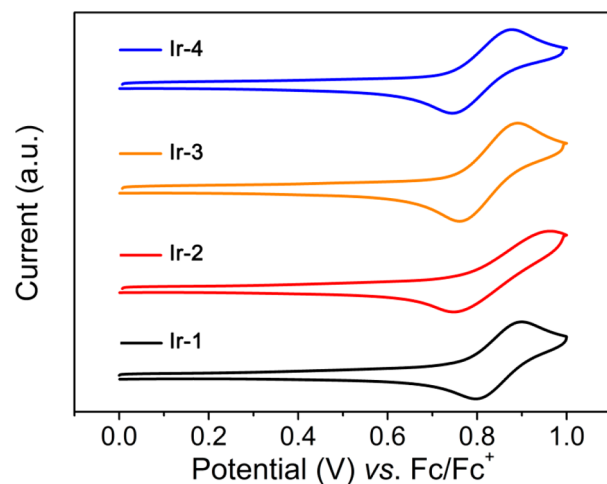


Figure 5. CV curves of Ir-1–Ir-4.

−3.02, −3.00, −3.10, and −3.04 eV, respectively, on the basis of the energy gaps.

Monochromatic OLED Characterization. To evaluate the EL performances of the designed iridium(III) complexes, the phosphorescent devices D1–D4 based on Ir-1–Ir-4 were fabricated with the same device structure of ITO/TAPC (4,4′-(cyclohexane-1,1-diyl)bis(*N,N*-di-*p*-tolylaniline, 35 nm)/TCTA (tris(4-(9*H*-carbazol-9-yl)phenyl)amine, 5 nm)/26DCzPPy (2,6-bis(3-(9*H*-carbazol-9-yl)phenyl)pyridine):Ir-1–Ir-4 (5 wt %, 20 nm)/TmPyPB (1,3,5-tris(3-pyridyl-3-phenyl)benzene, 40 nm)/LiF (0.5 nm)/Ag:Mg (1:15, 120 nm). LiF acts as the electron injection material. In addition, TAPC was used as the hole-transporting layer (HTL) because of its high hole mobility of $\sim 10^{-2} \text{ cm}^2 \text{ V}^{-1} \text{ s}^{-1}$, and TCTA served as a electron/exciton blocking layer (EBL). Furthermore, the bipolar material 26DCzPPy, which has equivalent electron and hole transport capabilities, was chosen as the host material.⁴⁷ TmPyPB acts as an electron-transporting layer (ETL).⁴⁸ Figure S7 in the Supporting Information shows the molecular structures of these materials. The corresponding EL characteristics and key data are shown in Figure 6 and Table 2.

As depicted in Figure 6b, devices D1 and D2 exhibit the same strong orange EL at 590 nm, with the same CIE coordinates of (0.53, 0.46). Furthermore, the EL spectra of the devices are in good agreement with those of the PL counterparts, indicating that the orange emission mainly comes from iridium(III) dopants. D3 and D4 show orange emission peaks at 590 and 625 nm and at 588 and 625 nm, respectively, with the same CIE coordinates of (0.60, 0.40). In addition, no significant emission from 26DCzPPy was observed in any spectra, indicating complete efficient energy transfer from 26DCzPPy to the iridium(III) dopants during

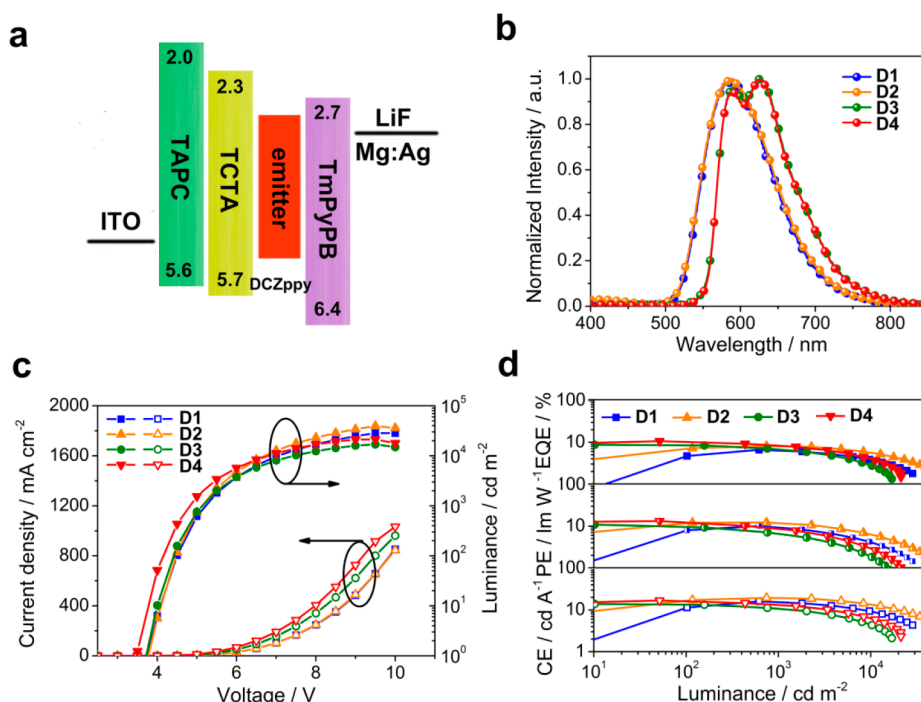


Figure 6. (a) Schematic energy-level diagram of monochromatic OLEDs. (b) EL spectra for monochromatic OLEDs. (c) Current density and luminance characteristics of monochromatic OLEDs. (d) CE, PE, and EQE curves of monochromatic OLEDs.

Table 2. EL Performance of OLEDs Based on Ir-1–Ir-4

device	$V_{\text{turn-on}}^a$ (V)	λ_{EL} (nm)	L_{max}^b (cd m^{-2})	$\text{CE}^{b,c}$ (cd A^{-1})	$\text{PE}^{b,c}$ (lm W^{-1})	$\text{EQE}^{b,c}$	CIE [(x, y), 70]
D1	3.8	590	28440	16.1, 15.7	10.1, 9.3	6.6, 6.3	(0.53, 0.46), 7.0
D2	3.8	590	39420	19.5, 19.2	12.2, 11.9	8.1, 8.0	(0.53, 0.46), 7.0
D3	3.7	590, 625	16930	13.9, 10.5	10.9, 6.5	8.7, 6.8	(0.60, 0.40), 7.0
D4	3.5	588, 625	21260	16.9, 13.2	13.3, 8.5	10.6, 8.2	(0.60, 0.40), 7.0
D5 ^d	3.1	581	38799	27.2, 24.3	24.0, 14.8	10.6, 9.4	(0.52, 0.47), 7.0
D6 ^e	3.5	581	31274	22.2, 20.4	17.4, 12.0	8.7, 8.0	(0.52, 0.47), 7.0

^aDriving voltages at 1 cd m^{-2} . ^bMaximum values (luminance, current efficiency, power efficiency, external quantum efficiency). ^cEfficiency values at 1000 cd m^{-2} . ^dOptimized device based on Ir-1. ^eOptimized device based on Ir-2.

electroluminescence.^{49–52} Here, the four orange devices also possess broad FWHMs of 107 nm for device D1, 109 nm for device D2, and 110 nm for devices D3 and D4, which are very favorable for the development of outstanding color quality WOLEDs.²⁶ These orange devices can be driven at low voltages from 3.5 to 3.8 V. Figure 6c,d exhibits the EL performance of the four devices. As shown in Table 2, devices D1 and D2 have better performance with maximum luminances of 28440 cd m^{-2} for D1 and 39420 cd m^{-2} for D2, maximum CEs of 16.1 cd A^{-1} for D1 and 19.5 cd A^{-1} for D2, maximum PEs of 10.1 lm W^{-1} for D1 and 12.2 lm W^{-1} for D2, peak EQEs of 6.6% for D1 and 8.1% for D2. Although the maximum PEs and EQEs of D3 and D4 have better results (10.9 and 13.3 lm W^{-1} , 8.7% and 10.6%) in comparison D1 and D2, D3 and D4 exhibit lower performance in the maximum luminance and maximum CE (16930 and 21260 cd m^{-2} , 13.9 and 16.9 cd A^{-1}). In addition, devices D1 and D2 show tiny CE efficiency roll-offs of 2.5% and 1.5%, respectively, outperforming the CE efficiency roll-offs of D3 and D4 (24.5% and 21.9%). Encouraged by the better EL performances of Ir-1 and Ir-2, the optimized devices D5 and D6 were prepared. MoO₃, which act as a hole injection material, was introduced,⁵³ and Bphen (4,7-diphenyl-1,10-phenanthroline) replaced TmPyPB as the new electron-transporting layer during the

optimization process. As shown in Figure S8c in the Supporting Information, the two orange devices exhibit maximum luminances of 38799 cd m^{-2} for D5 and 31274 cd m^{-2} for D6. From Figure S4d in the Supporting Information, the efficiency of D5 attained a peak CE of 27.2 cd A^{-1} , a peak PE of 24.0 lm W^{-1} , and a peak EQE of 10.6%, respectively. Relative to D5, D6 shows slightly lower efficiencies for a maximum CE of 22.2 cd A^{-1} , a maximum PE of 17.4 lm W^{-1} , and a maximum EQE of 8.7%. In addition, the two devices both show low CE and EQE efficiency roll-offs. They retained CE and EQE values of 24.3 cd A^{-1} , 9.4% for D5 and 20.4 cd A^{-1} and 8.0% for D6 at a luminance of 1000 cd m^{-2} , suggesting a well-balanced charge-transport characteristic in the devices.⁵⁴ The excellent performances of devices D1, D2, D5, and D6 indicate that Ir-1 and Ir-2 can act as efficient orange emitters for efficient white OLEDs.⁵⁵

WOLED Characterization. Encouraged by the broad FWHMs and high efficiency of the monochromatic devices, warm WOLEDs which comprise blue and orange emitters were prepared with the structure ITO/MoO₃ (3 nm)/TAPC (4,4'-(cyclohexane-1,1-diyl)bis(*N,N*-di-*p*-tolylaniline), 35 nm)/TCTA ((tris(4-(9*H*-carbazol-9-yl)phenyl)amine), 5 nm)/26DCZPPy (2,6-bis(3-(9*H*-carbazol-9-yl)phenyl)pyridine):FIrpic (10%, 5 nm)/26DCZPPy:Ir-1 (W1) and Ir-

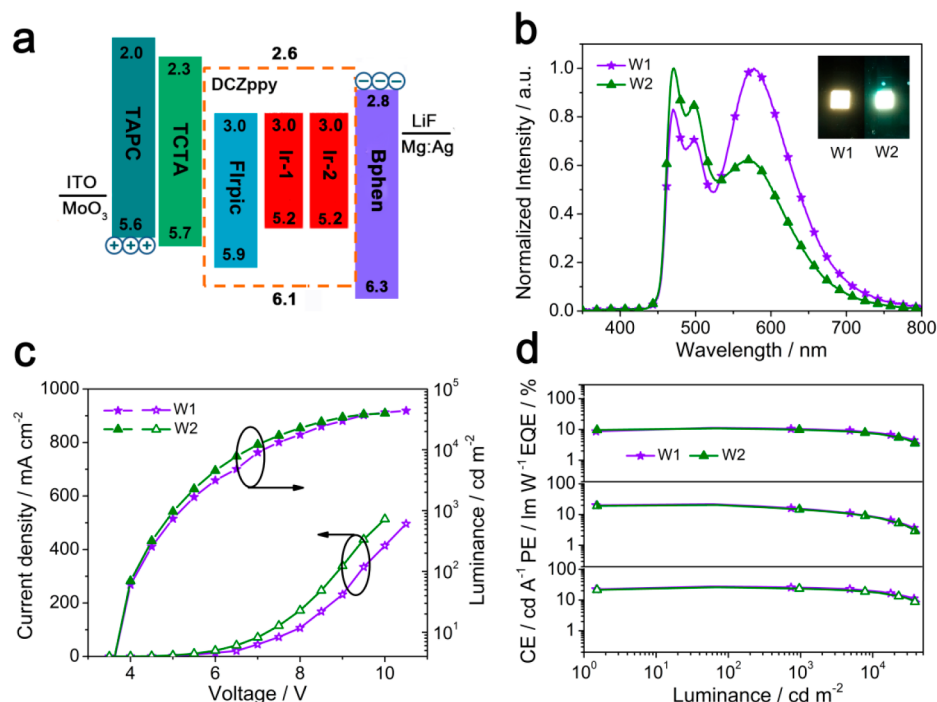


Figure 7. (a) Schematic energy-level diagram of two-color warm WOLEDs. (b) EL spectra for two-color warm WOLEDs. (c) Current density and luminance characteristics of two-color warm WOLEDs. (d) CE, PE, and EQE curves of two-color warm WOLEDs.

Table 3. EL Performance of White OLEDs Based on Ir-1 and Ir-2

device	$V_{\text{turn-on}}^a$ (V)	L_{max}^b (cd m ⁻²)	CE ^{b,c} (cd A ⁻¹)	PE ^{b,c} (lm W ⁻¹)	EQE ^{b,c}	CRI	CIE [(x, y), V]
W1	3.3	43980	27.7, 25.5	21.8, 15.7	11.3, 10.4	69	(0.39, 0.43), 7.0
W2	3.3	39811	26.1, 23.6	20.5, 14.8	10.9, 9.9	67	(0.32, 0.41), 7.0

^aDriving voltages at 1 cd m⁻². ^bMaximum values (luminance, current efficiency, power efficiency, external quantum efficiency). ^cEfficiency values at 1000 cd m⁻².

2 (W2) (7%, 15 nm)/Bphen (4,7-diphenyl-1,10-phenanthroline, 40 nm)/LiF (0.5 nm)/Ag:Mg (1:15, 120 nm). Figure 7a displays the schematic energy-level diagram. The HOMO and LUMO energy levels of Ir-1 and Ir-2 were embedded between the HOMO and LUMO levels of 26DCzPPy, which is expected to have good carrier-trapping performance. In addition, significantly different energy levels between the emitters and the host indicate efficient energy transfer from 26DCzPPy to the dopants. Furthermore, TCTA not only facilitates hole injection but also acts as an electron-blocking layer to block the migration of electrons from the host material, making carriers well confined within the emitting layers (EML). The EL spectra, current density, luminance characteristics, and CE, PE, and EQE curves for two-color warm WOLEDs are illustrated in Figure 7, and related EL data are given in Table 3.

From Figure 7b, two main emission peaks (470 and 577 nm for W1, 471 and 569 nm for W2) which can be observed from the EL spectra of W1 and W2 correspond to emissions of FIrpic and Ir-1 and Ir-2. In addition, the main emission intensity is located at the orange band in EL spectra, which makes the device W1 have a lower correlated color temperature (CCT) of 4024 K in comparison to W2 (5709 K) at 6 V.⁵⁶ W1 shows warm white emission with CIE coordinates of (0.39, 0.43) at 7 V. It is worth mentioning that W1 also displays excellent color stability. When the voltage changes from 4 to 6 V, the CIE coordinates change slightly from (0.392, 0.432) to (0.395, 0.433) (Figure 8). Additionally,

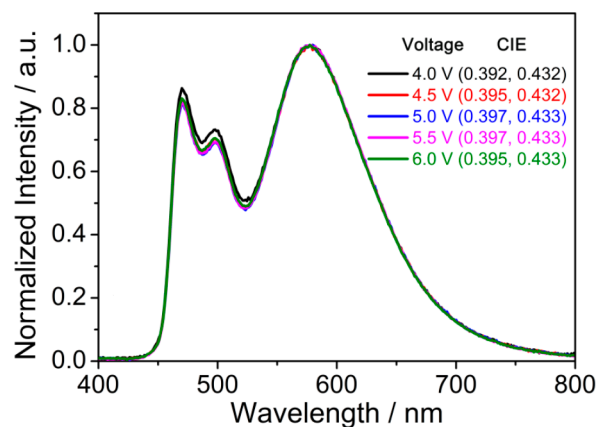


Figure 8. EL spectra of a WOLED (W1) with the designed emitter Ir-1 at various voltages.

the CIE coordinates of W2 remain almost invariable when the voltage goes from 4 V (0.321, 0.414) to 6 V (0.326, 0.415) (see Figure S9 in the Supporting Information). However, WOLEDs have a lower color rendering index (CRI) of 69 for W1 and 67 for W2, which probably is due to limited blue-emitting spectra not covering the whole spectral region well.²⁶ Due to the good matching of the energy levels, W1 and W2 have the same low turn-on voltage of 3.3 V. The devices W1 and W2 reach maximum luminances of 43980 and 39811 cd m⁻², respectively (Figure 7c). As depicted in Figure 7d, a

maximum CE of 27.7 cd A⁻¹, PE of 21.8 lm W⁻¹, and EQE of 11.3% are realized in **W1**. The performance of **W2** has a slight drop in comparison with **W1**, which possesses a maximum CE of 26.1 cd A⁻¹, PE of 20.5 lm W⁻¹, and EQE of 10.9%. Importantly, both **W1** and **W2** show negligible CE and EQE efficiency roll-offs. At a luminance of 1000 cd m⁻², CE and EQE of **W1** are still maintained at 25.5 cd A⁻¹ and 10.4%, respectively, revealing an attenuation of about 7.9% and 8.0% relative to the maximum value. For **W2**, CE and EQE declined to 23.6 cd A⁻¹ and 9.9% when the luminance was 1000 cd m⁻².

CONCLUSIONS

In summary, the four efficient orange iridium complexes **Ir-1**–**Ir-4** were successfully designed and synthesized, of which **Ir-1** and **Ir-2** had PLQYs of 57.5% and 56.4%, respectively. The corresponding OLEDs based on these complexes have broad FWHMs of about 110 nm. The optimized device **D5** based on **Ir-1** achieved the best performance with a maximum CE of 27.2 cd A⁻¹, PE of 24.0 lm W⁻¹, and EQE of 10.6%. The corresponding two-color warm WOLED comprising **Ir-1** as the orange dopant achieves a maximum brightness of 43980 cd m⁻², a peak CE of 27.7 cd A⁻¹, a peak PE of 21.8 lm W⁻¹, and a peak EQE of 11.3% accompanied by a small CE roll-off of 7.9%. Importantly, the warm WOLED also displays excellent color stability with Δ CIE = (0.003, 0.001) when driving voltages were varied from 4 to 6 V. In view of the achieved high PLQYs and promising device efficiency associated with the tiny roll-off at high luminance, we believe that the two complexes have great prospects in the field of solid-state lighting and displays.

EXPERIMENTAL SECTION

General Information. All reagents and solvents used in the experiment were commercially available. The molecular weights of **Ir-1**–**Ir-4** were measured by using a matrix-assisted laser desorption ionization time-of-flight (MALDI-TOF) mass spectrometer. Photoluminescence (PL) emission spectra of emitters were recorded by using a FL-4600 fluorescent spectrophotometer. UV–vis absorption spectra of emitters were tested on a Cary 500 UV–vis–NIR spectrophotometer, and lifetimes were performed with an Edinburgh FLS920 spectrofluorimeter at room temperature. The spin-coating method was used to fabricate the neat films. Cyclic voltammetry (CV) investigations were conducted on a workstation (BAS 100 W instrument) using dichloromethane or acetonitrile containing 0.1 M *n*-Bu₄NPF₆ as a supporting electrolyte under a N₂ atmosphere. The ferrocene/ferrocenium (Fc/Fc⁺) couple was chosen for calibration. PLQYs in solution were measured on a C9920-02 system under a N₂ atmosphere. PLQYs in neat films were measured in an integrating sphere.

Synthesis of 2-(1*H*-Benzo[d]imidazol-2-yl)quinolone (HBIQ) and 1-(1*H*-Benzo[d]imidazol-2-yl)isoquinoline (HBISQ). The preparations of HBIQ and HBISQ are given in previously reported literature.⁵⁷

Synthesis of 1-Phenyl-2-*p*-tolyl-1*H*-benzo[d]imidazole (HmPBI). A 50.00 mmol amount (9.21 g) of *N*-phenyl-*o*-phenylenediamine was dissolved in 30 mL of *N,N*-dimethylacetamide. Under nitrogen, 20 mL of an *N,N*-dimethylacetamide solution of 4-methylbenzoyl chloride (50.00 mmol, 7.73 g) was slowly added dropwise to the above solution and stirred at room temperature for 2 h. After the reaction, a large amount of water was added to obtain a solid. After washing and drying, the resulting intermediate was added to 20 mL of glacial acetic acid and refluxed for 16 h. Water was added to obtain the product after the mixture was cooled to 25 °C. Then, the product was purified by silica gel column chromatography. ¹H NMR (500 MHz, CDCl₃, δ): 7.89 (d, *J* = 8.0 Hz, 1H), 7.52–7.45 (m,

5H), 7.35–7.31 (m, 3H), 7.27–7.23 (m, 2H), 7.11 (d, *J* = 8.0 Hz, 2H), 2.34 (s, 3H).

Synthesis of 2-(4-*tert*-Butylphenyl)-1-phenyl-1*H*-benzo[d]imidazole (HtbPBI). The synthesis of HtbPBI was similar to that of HmPBI with 4-*tert*-butylbenzoyl chloride as the starting material. ¹H NMR (500 MHz, CDCl₃, δ): 7.88 (d, *J* = 8.0 Hz, 1H), 7.53–7.48 (m, 5H), 7.35–7.30 (m, 5H), 7.26–7.21 (m, 2H), 1.29 (s, 9H).

Synthesis of Dichloro-Bridged Diiridium Complex [Ir(mPBI)₂Cl]₂. IrCl₃·3H₂O (1.06 g, 3.00 mmol), HmPBI (2.05 g, 7.20 mmol), 2-ethoxyethanol (60 mL), and water (20 mL) were mixed together and refluxed under argon for 24 h. The reaction mixture was then cooled to 25 °C and filtered. After washing and drying, the product was collected.

Synthesis of [Ir(tbPBI)₂Cl]₂. The synthetic method of [Ir(tbPBI)₂Cl]₂ is similar to that of [Ir(mPBI)₂Cl]₂, in which the HmPBI is replaced by HtbPBI.

Synthesis of Ir-1. The ancillary ligand HBIQ (0.15 g, 0.60 mmol), dichloro-bridged diiridium complex [Ir(mPBI)₂Cl]₂ (0.38 g, 0.24 mmol), and K₂CO₃ (0.08 g, 0.60 mmol) were dissolved in dichloromethane (60 mL) and ethanol (20 mL). Then the mixture was refluxed for 24 h under the protection of argon in the dark. After it was cooled to room temperature, the mixture was distilled off the solvent, and then the crude product was purified through silica gel column chromatography to afford complex **Ir-1** in 68% yield. ¹H NMR (600 MHz, DMSO-*d*₆, δ): 8.65 (s, 2H), 8.12 (d, *J* = 9.0 Hz, 1H), 8.04 (d, *J* = 7.8 Hz, 1H), 7.71–7.80 (m, 7H), 7.52–7.56 (m, 4H), 7.30 (s, 1H), 7.03–7.15 (m, 6H), 6.71–6.94 (m, 2H), 6.62 (d, *J* = 8.4 Hz, 2H), 6.54 (d, *J* = 8.4 Hz, 1H), 6.45–6.49 (m, 2H), 6.40 (s, 1H), 6.22 (s, 1H), 5.95 (d, *J* = 8.4 Hz, 1H), 5.91 (d, *J* = 7.8 Hz, 1H), 5.43 (d, *J* = 8.4 Hz, 1H), 2.07 (s, 3H), 2.03 (s, 3H). MS (MALDI-TOF, *m/z*): 1004.3 [M + H]⁺.

Synthesis of Ir-2. The synthetic method of **Ir-2** is similar to that of **Ir-1**, in which the dichloro-bridged diiridium complex [Ir(mPBI)₂Cl]₂ is replaced by [Ir(tbPBI)₂Cl]₂. Yield: 67%. ¹H NMR (600 MHz, DMSO-*d*₆, δ): 8.72 (s, 2H), 8.04 (d, *J* = 7.2 Hz, 1H), 7.98 (d, *J* = 9.0 Hz, 1H), 7.74–7.80 (m, 7H), 7.66–7.67 (m, 2H), 7.50 (s, 1H), 7.31 (d, *J* = 5.4 Hz, 1H), 7.26 (d, *J* = 6.6 Hz, 1H), 7.07–7.14 (m, 3H), 6.98–7.02 (m, 3H), 6.86 (d, *J* = 8.4 Hz, 1H), 6.77–6.81 (m, 2H), 6.73 (s, 1H), 6.59 (s, 1H), 6.45–6.50 (m, 3H), 6.35 (s, 1H), 6.06 (d, *J* = 8.4 Hz, 1H), 5.59 (d, *J* = 7.8 Hz, 1H), 5.46 (s, 1H), 0.93 (s, 9H), 0.87 (s, 9H). MS (MALDI-TOF, *m/z*): 1088.4 [M + H]⁺.

Synthesis of Ir-3. The synthetic method of **Ir-3** is similar to that of **Ir-1**, in which the ancillary ligand HBIQ is replaced by HBISQ. Yield: 63%. ¹H NMR (600 MHz, DMSO-*d*₆, δ): 10.79 (s, 1H), 8.05–8.07 (m, 2H), 7.71–7.93 (m, 11H), 7.58 (t, *J* = 3.6 Hz, 2H), 7.45 (d, *J* = 6.0 Hz, 1H), 6.95–7.10 (m, 5H), 6.81 (t, *J* = 7.8 Hz, 1H), 6.73 (s, 1H), 6.69 (t, *J* = 7.5 Hz, 1H), 6.49–6.58 (m, 4H), 6.37 (d, *J* = 13.2 Hz, 2H), 6.26 (d, *J* = 8.4 Hz, 1H), 5.83 (d, *J* = 8.4 Hz, 1H), 5.64 (d, *J* = 4.8 Hz, 1H), 2.03 (d, *J* = 9.0 Hz, 6H). MS (MALDI-TOF, *m/z*): 1004.3 [M + H]⁺.

Synthesis of Ir-4. The synthetic method of **Ir-4** is similar to that of **Ir-2**, in which the ancillary ligand HBIQ is replaced by HBISQ. Yield: 62%. ¹H NMR (600 MHz, DMSO-*d*₆, δ): 10.86 (s, 1H), 8.05 (d, *J* = 7.2 Hz, 1H), 7.98 (d, *J* = 6.0 Hz, 1H), 7.92–7.94 (m, 2H), 7.70–7.85 (m, 10H), 7.27–7.32 (m, 2H), 7.14–7.15 (m, 1H), 7.06–7.09 (m, 2H), 6.99 (d, *J* = 8.4 Hz, 2H), 6.91 (t, *J* = 7.8 Hz, 1H), 6.79–6.81 (m, 1H), 6.75–6.76 (m, 1H), 6.72 (t, *J* = 7.8 Hz, 1H), 6.58–6.60 (m, 2H), 6.47–6.52 (m, 3H), 5.97–6.00 (m, 2H), 5.75–5.76 (m, 1H), 0.89 (d, *J* = 7.2 Hz, 18H). MS (MALDI-TOF, *m/z*): 1088.4 [M + H]⁺.

Single-Crystal X-ray Diffraction Analysis. Single crystals of **Ir-1**, **Ir-3**, and **Ir-4** were grown from mixed solution of CH₂Cl₂ and CH₃OH by slowly evaporating the solutions. The single-crystal X-ray diffraction data for the complexes were confirmed on a Bruker Apex CCD II area-detector diffractometer.

Computational Details. Theoretical calculations on **Ir-1**–**Ir-4** were performed with the Gaussian 09 software package.⁵⁸ The ground-state (S₀) and triplet-state (T₁) structures of the phosphors were fully optimized with B3LYP spin-unrestricted open-shell B3LYP, respectively. The standard 6-31G(d,p) basis set was used for C, H,

and N atoms, and the LANL2DZ basis set was employed for the iridium(III) atom in all calculations.

■ ASSOCIATED CONTENT

Supporting Information

The Supporting Information is available free of charge at <https://pubs.acs.org/doi/10.1021/acs.organomet.0c00472>.

OLED fabrication and measurements and figures and calculated energy levels of the lower-lying transitions of all complexes (PDF)

Accession Codes

CCDC 1969397 and 1980337–1980338 contain the supplementary crystallographic data for this paper. These data can be obtained free of charge via www.ccdc.cam.ac.uk/data_request/cif, or by emailing data_request@ccdc.cam.ac.uk, or by contacting The Cambridge Crystallographic Data Centre, 12 Union Road, Cambridge CB2 1EZ, UK; fax: +44 1223 336033.

■ AUTHOR INFORMATION

Corresponding Authors

Guo-Gang Shan – Institute of Functional Material Chemistry and National & Local United Engineering Lab for Power Battery, Faculty of Chemistry, Northeast Normal University, Changchun 130024, People's Republic of China; orcid.org/0000-0002-1050-219X; Phone: +86-431-85099108; Email: shangg187@nenu.edu.cn; Fax: +86-431-85684009

Hai-Zhu Sun – Institute of Functional Material Chemistry and National & Local United Engineering Lab for Power Battery, Faculty of Chemistry, Northeast Normal University, Changchun 130024, People's Republic of China; orcid.org/0000-0002-5113-8267; Email: sunhz335@nenu.edu.cn

Wen-Fa Xie – State Key Laboratory on Integrated Optoelectronics, College of Electronic Science and Engineering, Jilin University, Changchun, Jilin 130012, People's Republic of China; orcid.org/0000-0003-0912-8046; Phone: +86-13844907598; Email: xiewf@jlu.edu.cn

Zhong-Min Su – Institute of Functional Material Chemistry and National & Local United Engineering Lab for Power Battery, Faculty of Chemistry, Northeast Normal University, Changchun 130024, People's Republic of China; School of Chemistry & Environmental Engineering, Changchun University of Science and Technology, Changchun, Jilin 130012, People's Republic of China; orcid.org/0000-0002-3342-1966; Email: zmsu@nenu.edu.cn

Authors

Lei Ding – Institute of Functional Material Chemistry and National & Local United Engineering Lab for Power Battery, Faculty of Chemistry, Northeast Normal University, Changchun 130024, People's Republic of China

Chun-Xiu Zang – State Key Laboratory on Integrated Optoelectronics, College of Electronic Science and Engineering, Jilin University, Changchun, Jilin 130012, People's Republic of China

Li-Li Wen – Institute of Functional Material Chemistry and National & Local United Engineering Lab for Power Battery, Faculty of Chemistry, Northeast Normal University, Changchun 130024, People's Republic of China

Ying Gao – Jilin Engineering Normal University, Changchun 130052, People's Republic of China

Complete contact information is available at:

<https://pubs.acs.org/doi/10.1021/acs.organomet.0c00472>

Notes

The authors declare no competing financial interest.

■ ACKNOWLEDGMENTS

The authors gratefully acknowledge financial support from the National Natural Science Foundation of China (21303012, 51902124 and 61474054), the Fundamental Research Funds for the Central Universities (2412019FZ012 and 2412019QD007), and the China Postdoctoral Science Foundation funded project (2019M651184).

■ REFERENCES

- (1) Gomez-Bombarelli, R.; Aguilera-Iparraguirre, J.; Hirzel, T. D.; Duvenaud, D.; Maclaurin, D.; Blood-Forsythe, M. A.; Chae, H. S.; Einzinger, M.; Ha, D. G.; Wu, T.; Markopoulos, G.; Jeon, S.; Kang, H.; Miyazaki, H.; Numata, M.; Kim, S.; Huang, W.; Hong, S. L.; Baldo, M.; Adams, R. P.; Aspuru-Guzik, A. Design of efficient molecular organic light-emitting diodes by a high-throughput virtual screening and experimental approach. *Nat. Mater.* **2016**, *15*, 1120–1127.
- (2) Xiao, L.; Chen, Z.; Qu, B.; Luo, J.; Kong, S.; Gong, Q.; Kido, J. Recent progresses on materials for electrophosphorescent organic light-emitting devices. *Adv. Mater.* **2011**, *23*, 926–952.
- (3) Wu, T.-L.; Huang, M.-J.; Lin, C.-C.; Huang, P.-Y.; Chou, T.-Y.; Chen-Cheng, R.-W.; Lin, H.-W.; Liu, R.-S.; Cheng, C.-H. Diboron compound-based organic light-emitting diodes with high efficiency and reduced efficiency roll-off. *Nat. Photonics* **2018**, *12*, 235–240.
- (4) Yan, Z.-P.; Liao, K.; Han, H.-B.; Su, J.; Zheng, Y.-X.; Zuo, J.-L. Chiral iridium(III) complexes with four-membered Ir–S–P–S chelating rings for high-performance circularly polarized OLEDs. *Chem. Commun.* **2019**, *55*, 8215–8218.
- (5) Fleetham, T.; Li, G.; Li, J. Phosphorescent Pt(II) and Pd(II) Complexes for Efficient, High-Color-Quality, and Stable OLEDs. *Adv. Mater.* **2017**, *29*, 1601861.
- (6) Costa, R. D.; Orti, E.; Bolink, H. J.; Monti, F.; Accorsi, G.; Armaroli, N. Luminescent Ionic Transition-Metal Complexes for Light-Emitting Electrochemical Cells. *Angew. Chem., Int. Ed.* **2012**, *51*, 8178–8211.
- (7) Pashaei, B.; Karimi, S.; Shahroosvand, H.; Abbasi, P.; Pilkington, M.; Bartolotta, A.; Fresta, E.; Fernandez-Cestau, J.; Costa, R. D.; Bonaccorso, F. Polypyridyl ligands as a versatile platform for solid-state light-emitting devices. *Chem. Soc. Rev.* **2019**, *48*, 5033–5139.
- (8) Lee, J.; Chen, H.-F.; Batagoda, T.; Coburn, C.; Djurovich, P. I.; Thompson, M. E.; Forrest, S. R. Deep blue phosphorescent organic light-emitting diodes with very high brightness and efficiency. *Nat. Mater.* **2016**, *15*, 92–98.
- (9) Fan, C.; Yang, C. Yellow/orange emissive heavy-metal complexes as phosphors in monochromatic and white organic light-emitting devices. *Chem. Soc. Rev.* **2014**, *43*, 6439–69.
- (10) Zhu, Y.-C.; Zhou, L.; Li, H.-Y.; Xu, Q.-L.; Teng, M.-Y.; Zheng, Y.-X.; Zuo, J.-L.; Zhang, H.-J.; You, X.-Z. Highly Efficient Green and Blue-Green Phosphorescent OLEDs Based on Iridium Complexes with the Tetraphenylimidodiphosphinate Ligand. *Adv. Mater.* **2011**, *23*, 4041–4046.
- (11) Fukagawa, H.; Oono, T.; Iwasaki, Y.; Hatakeyama, T.; Shimizu, T. High-efficiency ultrapure green organic light-emitting diodes. *Mater. Chem. Front.* **2018**, *2*, 704–709.
- (12) Sree, V. G.; Maheshwaran, A.; Kim, H.; Park, H.-Y.; Kim, Y.; Lee, J. C.; Song, M.; Jin, S.-H. Synthesis and Characterization of Highly Efficient Solution-Processable Green Ir(III) Complexes with High Current Efficiency and Very Low Efficiency Roll-Off. *Adv. Funct. Mater.* **2018**, *28*, 1804714.
- (13) Hao, Z.; Zhang, K.; Wang, P.; Lu, X.; Lu, Z.; Zhu, W.; Liu, Y. Deep Red Iridium(III) Complexes Based on Pyrene-Substituted Quinoxaline Ligands for Solution-Processed Phosphorescent Organic Light-Emitting Diodes. *Inorg. Chem.* **2020**, *59*, 332–342.
- (14) Xu, T.; Zhang, Y.-X.; Wang, B.; Huang, C.-C.; Murtaza, I.; Meng, H.; Liao, L.-S. Highly Simplified Reddish Orange Phosphorescent Organic Light-Emitting Diodes Incorporating a Novel Carrier

and Exciton-Confining Spiro-Exciplex-Forming Host for Reduced Efficiency Roll-off. *ACS Appl. Mater. Interfaces* **2017**, *9*, 2701–2710.

(15) Yan, Z.; Wang, Y.; Ding, J.; Wang, Y.; Wang, L. Highly Efficient Phosphorescent Furo[3,2-c]pyridine Based Iridium Complexes with Tunable Emission Colors over the Whole Visible Range. *ACS Appl. Mater. Interfaces* **2018**, *10*, 1888–1896.

(16) Zhou, W.; Wang, Z.; Zhang, J.; Hu, S.; Xie, Q.; Liu, Z.; Liu, L.; Liang, A. Orange-emitting supramolecular phosphorescent polymer with different counterions for polymer light-emitting diodes. *Dyes Pigm.* **2020**, *172*, 107790.

(17) Reineke, S.; Lindner, F.; Schwartz, G.; Seidler, N.; Walzer, K.; Lussem, B.; Leo, K. White organic light-emitting diodes with fluorescent tube efficiency. *Nature* **2009**, *459*, 234–238.

(18) Farinola, G. M.; Ragni, R. Electroluminescent materials for white organic light emitting diodes. *Chem. Soc. Rev.* **2011**, *40*, 3467–3482.

(19) Kamtekar, K. T.; Monkman, A. P.; Bryce, M. R. Recent advances in white organic light-emitting materials and devices (WOLEDs). *Adv. Mater.* **2010**, *22*, 572–582.

(20) Schwartz, G.; Reineke, S.; Rosenow, T. C.; Walzer, K.; Leo, K. Triplet Harvesting in Hybrid White Organic Light-Emitting Diodes. *Adv. Funct. Mater.* **2009**, *19*, 1319–1333.

(21) Dai, X.; Yao, F.; Li, J.; Yu, H.; Cao, J. Color-stable non-doped white phosphorescent organic light-emitting diodes based on ultrathin emissive layers. *J. Phys. D: Appl. Phys.* **2020**, *53*, 055106.

(22) Chen, Z.; Ho, C. L.; Wang, L.; Wong, W. Y. Single-Molecular White-Light Emitters and Their Potential WOLED Applications. *Adv. Mater.* **2020**, *32*, 1903269.

(23) Kuei, C. Y.; Tsai, W. L.; Tong, B.; Jiao, M.; Lee, W. K.; Chi, Y.; Wu, C. C.; Liu, S. H.; Lee, G. H.; Chou, P. T. Bis-Tridentate Ir(III) Complexes with Nearly Unitary RGB Phosphorescence and Organic Light-Emitting Diodes with External Quantum Efficiency Exceeding 31%. *Adv. Mater.* **2016**, *28*, 2795–2800.

(24) Miao, Y.; Wang, K.; Zhao, B.; Gao, L.; Tao, P.; Liu, X.; Hao, Y.; Wang, H.; Xu, B.; Zhu, F. High-efficiency/CRI/color stability warm white organic light-emitting diodes by incorporating ultrathin phosphorescence layers in a blue fluorescence layer. *Nanophotonics* **2018**, *7*, 295–304.

(25) Sasabe, H.; Takamatsu, J.; Motoyama, T.; Watanabe, S.; Wagenblast, G.; Langer, N.; Molt, O.; Fuchs, E.; Lennartz, C.; Kido, J. High-efficiency blue and white organic light-emitting devices incorporating a blue iridium carbene complex. *Adv. Mater.* **2010**, *22*, 5003–5007.

(26) Tao, P.; Li, W.-L.; Zhang, J.; Guo, S.; Zhao, Q.; Wang, H.; Wei, B.; Liu, S.-J.; Zhou, X.-H.; Yu, Q.; Xu, B.-S.; Huang, W. Facile Synthesis of Highly Efficient Lepidine-Based Phosphorescent Iridium(III) Complexes for Yellow and White Organic Light-Emitting Diodes. *Adv. Funct. Mater.* **2016**, *26*, 881–894.

(27) Li, X.; Cui, J.; Ba, Q.; Zhang, Z.; Chen, S.; Yin, G.; Wang, Y.; Li, B.; Xiang, G.; Kim, K. S.; Xu, H.; Zhang, Z.; Wang, H. L. Multiphotoluminescence from a Triphenylamine Derivative and Its Application in White Organic Light-Emitting Diodes Based on a Single Emissive Layer. *Adv. Mater.* **2019**, *31*, 1900613.

(28) Yang, X.; Zhao, Y.; Zhang, X.; Li, R.; Dang, J.; Li, Y.; Zhou, G.; Wu, Z.; Ma, D.; Wong, W.-Y.; Zhao, X.; Ren, A.; Wang, L.; Hou, X. Thiazole-based metallophosphors of iridium with balanced carrier injection/transporting features and their two-colour WOLEDs fabricated by both vacuum deposition and solution processing-vacuum deposition hybrid strategy. *J. Mater. Chem.* **2012**, *22*, 7136–7148.

(29) Zhang, G. H.; Xie, F. M.; Wu, K.; Li, Y. Q.; Xie, G.; Zou, S. J.; Shen, Y.; Zhao, X.; Yang, C.; Tang, J. X. High-Efficiency White Organic Light-Emitting Diodes Based on All Nondoped Thermally Activated Delayed Fluorescence Emitters. *Adv. Mater. Interfaces* **2020**, *7*, 1901758.

(30) Tian, Q. S.; Zhang, L.; Hu, Y.; Yuan, S.; Wang, Q.; Liao, L. S. High-Performance White Organic Light-Emitting Diodes with Simplified Structure Incorporating Novel Exciplex-Forming Host. *ACS Appl. Mater. Interfaces* **2018**, *10*, 39116–39123.

(31) Yan, Z.; Wang, Y.; Wang, J.; Wang, Y.; Ding, J.; Wang, L. A novel furo[3,2-c]pyridine-based iridium complex for high-performance organic light-emitting diodes with over 30% external quantum efficiency. *J. Mater. Chem. C* **2017**, *5*, 10122–10125.

(32) Mondal, E.; Hung, W.-Y.; Dai, H.-C.; Wong, K.-T. Fluorene-Based Asymmetric Bipolar Universal Hosts for White Organic Light Emitting Devices. *Adv. Funct. Mater.* **2013**, *23*, 3096–3105.

(33) Wen, L.-L.; Zang, C.-X.; Gao, Y.; Shan, G.-G.; Sun, H.-Z.; Wang, T.; Xie, W.-F.; Su, Z.-M. Molecular Engineering of Phenylbenzimidazole-Based Orange Ir(III) Phosphors toward High-Performance White OLEDs. *Inorg. Chem.* **2018**, *57*, 6029–6037.

(34) Gong, S.; Chen, Y.; Yang, C.; Zhong, C.; Qin, J.; Ma, D. De Novo Design of Silicon-Bridged Molecule Towards a Bipolar Host: All-Phosphor White Organic Light-Emitting Devices Exhibiting High Efficiency and Low Efficiency Roll-Off. *Adv. Mater.* **2010**, *22*, 5370–5373.

(35) Guo, L. Y.; Zhang, X. L.; Wang, H. S.; Liu, C.; Li, Z. G.; Liao, Z. J.; Mi, B. X.; Zhou, X. H.; Zheng, C.; Li, Y. H.; Gao, Z. Q. New homoleptic iridium complexes with C^N = N type ligand for high efficiency orange and single emissive-layer white OLEDs. *J. Mater. Chem. C* **2015**, *3*, 5412–5418.

(36) Cao, H.; Shan, G.; Wen, X.; Sun, H.; Su, Z.; Zhong, R.; Xie, W.; Li, P.; Zhu, D. An orange iridium(III) complex with wide-bandwidth in electroluminescence for fabrication of high-quality white organic light-emitting diodes. *J. Mater. Chem. C* **2013**, *1*, 7371–7379.

(37) Jiang, B.; Zhao, C.; Ning, X.; Zhong, C.; Ma, D.; Yang, C. Using Simple Fused-Ring Thieno[2,3-d]pyrimidine to Construct Orange/Red Ir(III) Complexes: High-Performance Red Organic Light-Emitting Diodes with EQEs up to Nearly 28%. *Adv. Opt. Mater.* **2018**, *6*, 1800108.

(38) Na, H.; Teets, T. S. Highly Luminescent Cyclometalated Iridium Complexes Generated by Nucleophilic Addition to Coordinated Isocyanides. *J. Am. Chem. Soc.* **2018**, *140*, 6353–6360.

(39) Liang, B.; Yu, Z.; Zhuang, X.; Wang, J.; Wei, J.; Ye, K.; Zhang, Z.; Liu, Y.; Wang, Y. Achieving High-Performance Pure-Red Electrophosphorescent Iridium(III) Complexes based on Optimizing Ancillary Ligand. *Chem. - Eur. J.* **2020**, *26*, 4410–4418.

(40) Pal, A. K.; Krotkus, S.; Fontani, M.; Mackenzie, C. F. R.; Cordes, D. B.; Slawin, A. M. Z.; Samuel, I. D. W.; Zysman-Colman, E. High-Efficiency Deep-Blue-Emitting Organic Light-Emitting Diodes Based on Iridium(III) Carbene Complexes. *Adv. Mater.* **2018**, *30*, 1804231.

(41) Li, Q.; Shi, C.; Huang, M.; Wei, X.; Yan, H.; Yang, C.; Yuan, A. B- and N-embedded color-tunable phosphorescent iridium complexes and B-N Lewis adducts with intriguing structural and optical changes. *Chem. Sci.* **2019**, *10*, 3257–3263.

(42) Liu, X.; Yu, Z.; Yu, M.; Zhang, X.; Xu, Y.; Lv, P.; Chu, S.; Liu, C.; Lai, W. Y.; Huang, W. Iridium(III)-Complexed Polydendrimers for Inkjet-Printing OLEDs: The Influence of Solubilizing Steric Hindrance Groups. *ACS Appl. Mater. Interfaces* **2019**, *11*, 26174–26184.

(43) Yang, X.; Guo, H.; Liu, B.; Zhao, J.; Zhou, G.; Wu, Z.; Wong, W. Y. Diarylboron-Based Asymmetric Red-Emitting Ir(III) Complex for Solution-Processed Phosphorescent Organic Light-Emitting Diode with External Quantum Efficiency above 28%. *Adv. Sci.* **2018**, *5*, 1701067.

(44) Ma, D.; Liu, R.; Qiu, Y.; Duan, L. High-performance yellow- and orange-emitting diodes based on novel sublimable cationic iridium(III) complexes by ligand control. *J. Mater. Chem. C* **2018**, *6*, 5630–5638.

(45) Niu, Z.-G.; Han, H.-B.; Li, M.; Zhao, Z.; Chen, G.-Y.; Zheng, Y.-X.; Li, G.-N.; Zuo, J.-L. Tunable Emission Color of Iridium(III) Complexes with Phenylpyrazole Derivatives as the Main Ligands for Organic Light-Emitting Diodes. *Organometallics* **2018**, *37*, 3154–3164.

(46) Sun, Y.; Yang, X.; Feng, Z.; Liu, B.; Zhong, D.; Zhang, J.; Zhou, G.; Wu, Z. Highly Efficient Deep-Red Organic Light-Emitting Devices Based on Asymmetric Iridium(III) Complexes with the Thianthrene

5,5,10,10-Tetraoxide Moiety. *ACS Appl. Mater. Interfaces* **2019**, *11*, 26152–26164.

(47) Chaskar, A.; Chen, H. F.; Wong, K. T. Bipolar host materials: a chemical approach for highly efficient electrophosphorescent devices. *Adv. Mater.* **2011**, *23*, 3876–3895.

(48) Yu, Z.; Zhang, J.; Liu, S.; Zhang, L.; Zhao, Y.; Zhao, H.; Xie, W. High-Efficiency Blue Phosphorescent Organic Light-Emitting Devices with Low Efficiency Roll-Off at Ultrahigh Luminance by the Reduction of Triplet-Polaron Quenching. *ACS Appl. Mater. Interfaces* **2019**, *11*, 6292–6301.

(49) Udagawa, K.; Sasabe, H.; Igarashi, F.; Kido, J. Simultaneous Realization of High EQE of 30%, Low Drive Voltage, and Low Efficiency Roll-Off at High Brightness in Blue Phosphorescent OLEDs. *Adv. Opt. Mater.* **2016**, *4*, 86–90.

(50) Liang, X.; Zhang, F.; Yan, Z. P.; Wu, Z. G.; Zheng, Y.; Cheng, G.; Wang, Y.; Zuo, J. L.; Pan, Y.; Che, C. M. Fast Synthesis of Iridium(III) Complexes Incorporating a Bis(diphenylphosphorothioyl)-amide Ligand for Efficient Pure Green OLEDs. *ACS Appl. Mater. Interfaces* **2019**, *11*, 7184–7191.

(51) Lu, G. Z.; Zhu, Q.; Liu, L.; Wu, Z. G.; Zheng, Y. X.; Zhou, L.; Zuo, J. L.; Zhang, H. Pure Red Iridium(III) Complexes Possessing Good Electron Mobility with 1,5-Naphthyridin-4-ol Derivatives for High-Performance OLEDs with an EQE over 31%. *ACS Appl. Mater. Interfaces* **2019**, *11*, 20192–20199.

(52) You, C.; Liu, D.; Meng, F.; Wang, Y.; Yu, J.; Wang, S.; Su, S.; Zhu, W. Iridium(III) phosphors with rigid fused-heterocyclic chelating architectures for efficient deep-red/near-infrared emissions in polymer light-emitting diodes. *J. Mater. Chem. C* **2019**, *7*, 10961–10971.

(53) Liu, Y.; Nell, B.; Ortstein, K.; Wu, Z.; Karpov, Y.; Beryozkina, T.; Lenk, S.; Kiriy, A.; Leo, K.; Reineke, S. High Electron Affinity Molecular Dopant CN6-CP for Efficient Organic Light-Emitting Diodes. *ACS Appl. Mater. Interfaces* **2019**, *11*, 11660–11666.

(54) Jing, Y.-M.; Wang, F.-Z.; Zheng, Y.-X.; Zuo, J.-L. Efficient deep red electroluminescence of iridium(III) complexes with 2,3-diphenylquinoxaline derivatives and tetraphenylimidodiphosphinate. *J. Mater. Chem. C* **2017**, *5*, 3714–3724.

(55) Li, G.; Zhu, D.; Peng, T.; Liu, Y.; Wang, Y.; Bryce, M. R. Very High Efficiency Orange-Red Light-Emitting Devices with Low Roll-Off at High Luminance Based on an Ideal Host-Guest System Consisting of Two Novel Phosphorescent Iridium Complexes with Bipolar Transport. *Adv. Funct. Mater.* **2014**, *24*, 7420–7426.

(56) Miao, Y.; Tao, P.; Wang, K.; Li, H.; Zhao, B.; Gao, L.; Wang, H.; Xu, B.; Zhao, Q. Highly Efficient Red and White Organic Light-Emitting Diodes with External Quantum Efficiency beyond 20% by Employing Pyridylimidazole-Based Metallophosphors. *ACS Appl. Mater. Interfaces* **2017**, *9*, 37873–37882.

(57) Chen, T.-R. Synthesis, structure, and field-effect property of 2-(benzimidazol-2-yl) quinoline. *Mater. Lett.* **2005**, *59*, 1050–1052.

(58) Frisch, M. J.; Trucks, G. W.; Schlegel, H. B.; Scuseria, G. E.; Robb, M. A.; Cheeseman, J. R.; Scalmani, G.; Barone, V.; Mennucci, B.; Petersson, G. A.; Nakatsuji, H.; Caricato, M.; Li, X.; Hratchian, H. P.; Izmaylov, A. F.; Bloino, J.; Zheng, G.; Sonnenberg, J. L.; Hada, M.; Ehara, M.; Toyota, K.; Fukuda, R.; Hasegawa, J.; Ishida, M.; Nakajima, T.; Honda, Y.; Kitao, O.; Nakai, H.; Vreven, T.; Montgomery, J. A., Jr.; Peralta, J. E.; Ogliaro, F.; Bearpark, M.; Heyd, J. J.; Brothers, E.; Kudin, K. N.; Staroverov, V. N.; Keith, T.; Kobayashi, R.; Normand, J.; Raghavachari, K.; Rendell, A.; Burant, J. C.; Iyengar, S. S.; Tomasi, J.; Cossi, M.; Rega, N.; Millam, J. M.; Klene, M.; Knox, J. E.; Cross, J. B.; Bakken, V.; Adamo, C.; Jaramillo, J.; Gomperts, R.; Stratmann, R. E.; Yazyev, O.; Austin, A. J.; Cammi, R.; Pomelli, C.; Ochterski, J. W.; Martin, R. L.; Morokuma, K.; Zakrzewski, V. G.; Voth, G. A.; Salvador, P.; Dannenberg, J. J.; Dapprich, S.; Daniels, A. D.; Farkas, O.; Foresman, J. B.; Ortiz, J. V.; Cioslowski, J.; Fox, D. J. *Gaussian 09, Rev. D.01*; Gaussian, Inc.: Wallingford, CT, 2013.